



**HAL**  
open science

# Estimating wave energy flux from significant wave height and peak period

Nicolas Guillou

► **To cite this version:**

Nicolas Guillou. Estimating wave energy flux from significant wave height and peak period. Renewable Energy, 2020, 155, pp.1383-1393. 10.1016/j.renene.2020.03.124 . hal-02863302

**HAL Id: hal-02863302**

**<https://hal.science/hal-02863302>**

Submitted on 22 Aug 2022

**HAL** is a multi-disciplinary open access archive for the deposit and dissemination of scientific research documents, whether they are published or not. The documents may come from teaching and research institutions in France or abroad, or from public or private research centers.

L'archive ouverte pluridisciplinaire **HAL**, est destinée au dépôt et à la diffusion de documents scientifiques de niveau recherche, publiés ou non, émanant des établissements d'enseignement et de recherche français ou étrangers, des laboratoires publics ou privés.



Distributed under a Creative Commons Attribution - NonCommercial 4.0 International License

# Estimating wave energy flux from significant wave height and peak period

Nicolas Guillou<sup>a,\*</sup>

<sup>a</sup>*Cerema, Direction Eau Mer et Fleuves, Environnement et Risques, Laboratoire de Génie Côtier et Environnement (LGCE), 155 rue Pierre Bouguer, Technopôle Brest-Iroise, BP 5, 29280, Plouzané, France*

---

## Abstract

Optimum design and location of wave energy converters in the marine environment require accurate assessments of the spatio-temporal variability of the available wave energy flux. However, numerical hindcast databases (commonly exploited for these long-term evaluations) integrate a restricted number of parameters such as the significant wave height  $H_s$  or the peak period  $T_p$ . Computation of wave power density from hindcast database is thus conducted by relying on simplified formulations derived from approximations of the group velocity and the wave energy spectrum. The present investigation quantified the biases in wave power computation from two standard formulations, based on the energy period and the peak period, respectively. The analysis relied on NOAA observations in 17 locations of the North-West Atlantic, the Gulf of Mexico and the Caribbean Sea. Whereas the energy-period formulation was a very good approximation of the wave power density in deep waters, the peak-period formulation (with a default calibration coef-

---

\*Corresponding author

*Email address:* [nicolas.guillou@cerema.fr](mailto:nicolas.guillou@cerema.fr) (Nicolas Guillou)

ficient  $\alpha = 0.9$ ) overestimated locally, by more than 8%, the available wave energy flux. A refined distribution of  $\alpha$  against classes of  $H_s$  and  $T_p$  was established to reduce these differences, decreasing the relative difference from 9.9% to 0.3% off the Greater Antilles.

*Keywords:* wave energy converter; wave power; North-West Atlantic; Gulf of Mexico; Caribbean Sea; USA East Coast

---

## 1. Introduction

The exploitation of the wave resource has raised, over the last decades, significant interest and investment promoting technological developments with a wide range of energy converters tested and deployed in real sea conditions [1]. However, optimum design and location of devices in the marine environment require refined estimations of the available wave power density characterizing, in particular, its evolution on different timescales from monthly to annual periods [2]. These aspects are fundamental as the wave resource may show significant temporal variability liable to impact performances of machines between energetic and low-energetic seasons and years, and thus the computational investment and economical return of a wave energy project [3, 4].

As scarce observations were available in locations of interest, the investigation of wave power variability relied, most of the time, on regional numerical hindcast simulations based on third-generation spectral wave models that provided a continuous and consistent assessment of the wave energy climate on multi-decadal periods of time [2, 5, 6]. However, in many locations, due to limited storage space, the recorded historical and on going sea wave characteristics (at all computational grid nodes) were restricted to integrated wave parameters such as the significant wave height  $H_s$  or the statistical periods (peak or mean periods,  $T_p$  and  $T_m$ ) setting aside a detailed assessment of the wave energy spectrum and a computation of the available wave energy flux. This situation was typical of wave hindcast and reanalysis archives primary dedicated to produce statistics and trends of the wave climate in the coastal regions [7, 8]. In these situations, the available resource was es-

26 timated with simplified formulations that were derived from approximations  
27 of (i) the group velocity in deep waters and (ii) the wave energy spectrum  
28 based on standard shapes such as Pierson-Moskowitz [9] or JONSWAP [10].  
29 Following these assumptions, the wave energy flux was expressed as a func-  
30 tion of the significant wave height and statistical periods, and results were  
31 exploited to provide preliminary assessments of the long-term spatial and  
32 temporal variabilities of wave power density [11, 12, 13].

33 Nevertheless, these simplified formulations may present important biases  
34 in comparison with the power directly computed from the spectral energy  
35 density and the superposition of an infinite number of waves with different  
36 heights and frequencies [14, 15]. By exploiting wave observations along the  
37 Atlantic coast of the southeastern USA, Defne et al. [14] found that a for-  
38 mulation of wave power based on  $H_s$  and  $T_m$  overestimated the available  
39 wave energy density by 40%. More recently, Ozkan et al. [15] exhibited that  
40 a standard equation based on wave height and energy period  $T_e$  underesti-  
41 mated the available wave power by an average of 17% in the coastal region  
42 of the Florida Peninsula (USA).

43 Complementing these investigations, the present study estimated and an-  
44 alyzed the differences in wave power computations from simplified formula-  
45 tions by relying on long-term observations of the National Data Buoy Center  
46 (NDBC) [16] (National Oceanic and Atmospheric Administration - NOAA)  
47 in offshore waters of the North-West Atlantic (off the USA East Coast, the  
48 Bahamas, and the Greater and Lesser Antilles), and in the Gulf of Mexico  
49 and the Caribbean Sea (Fig. 1, Section 2.1). The investigation considered  
50 two standard formulations, widely-used in wave energy resource assessments

51 and based on the energy period and the peak period, respectively (Section  
 52 2.2). Results of these two formulations were compared to a direct compu-  
 53 tation of the wave power density from the observed spectral energy density  
 54 (Section 2.3). The analysis was successively dedicated to the estimation of  
 55 the averaged wave power and the differences at monthly, seasonal and an-  
 56 nual time scales (Sections 3.1 and 3.2). A refined distribution of a calibration  
 57 coefficient against classes of  $H_s$  and  $T_p$  was finally established to reduce the

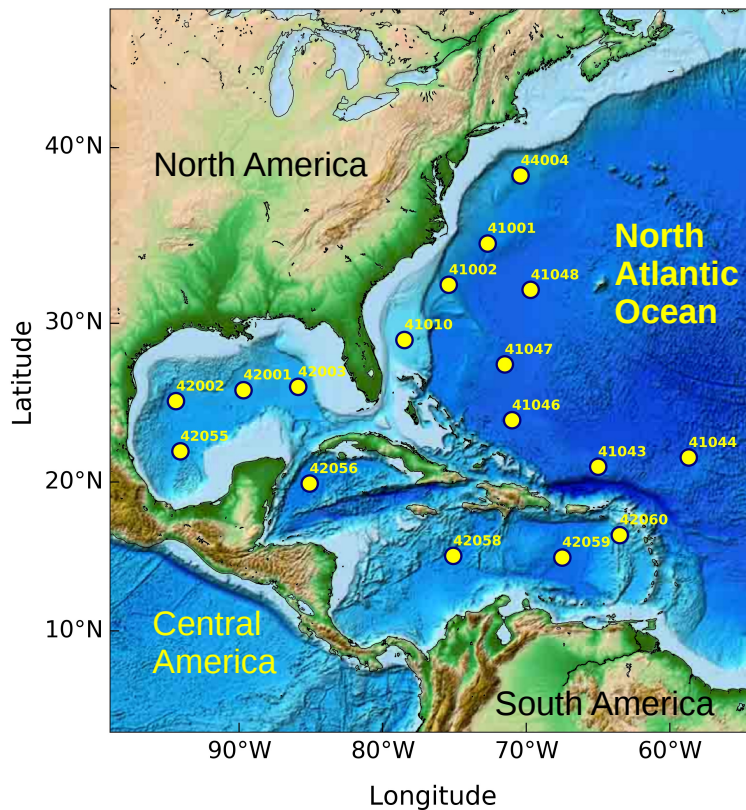


Figure 1: Locations of available wave buoys retained for the evaluation of the wave energy flux.

58 differences associated with the peak-period formulation (Section 3.3).

## 59 2. Materials and methods

### 60 2.1. Wave observations

61 Current study was conducted by exploiting wave energy spectrum mea-  
62 surements, available with a time step of one hour, in NDBC buoys of the  
63 North-West Atlantic Ocean [16]. The analysis was restricted to (i) loca-  
64 tions with mean water depths over 600 m in order to satisfy the deep water  
65 assumption described in Section 2.2, and (ii) observations that cover more  
66 than eight years so as to be able to characterize the seasonal and annual  
67 variabilities in wave power. This selection resulted in a series of 17 locations  
68 disseminated in offshore waters off the USA East Coast, the Bahamas, the  
69 Greater and Lesser Antilles, the Caribbean Sea and the Gulf of Mexico (Fig.  
70 1, Table 1).

### 71 2.2. Wave power formulations

72 The available wave energy flux, also denoted the wave power density or  
73 wave energy potential ( $\text{Wm}^{-1}$ , per unit length of wave front) is commonly  
74 evaluated as the integral of the product between the group velocity  $c_g$  and  
75 the spectral energy density  $E$  ( $\text{m}^2 \text{s}^{-1}$ ) with the following relationship

$$P_{\text{spectral}} = \rho g \int_0^{\infty} c_g(f) E(f) df \quad (1)$$

76 where  $f$  is the individual wave frequency,  $\rho$  is the density of sea water taken  
77 here equal to  $\rho = 1025 \text{ kg m}^{-3}$  and  $g$  is the gravity acceleration taken equal  
78 to  $g = 9.81 \text{ m s}^{-2}$ . The group velocity that accounts for the phase speed of

Table 1: Measurement points considered for the evaluation of the available wave energy flux.

Wave buoys	Coordinates		Water depth (m)	Duration (years)
	Lon.	Lat.		
41001	72.7° W	34.7° N	4479	20
41002	75.4° W	32.3° N	3680	21
41010	78.5° W	29.0° N	895	22
41043	65.0° W	21.0° N	5364	11
41044	58.7° W	21.6° N	5413	9
41046	71.0° W	24.0° N	5523	11
41047	71.5° W	27.5° N	5313	11
41048	69.7° W	32.0° N	5374	11
42001	89.7° W	25.9° N	3208	22
42002	94.4° W	25.2° N	3614	22
42003	85.9° W	26.1° N	3246	22
42055	94.1° W	22.0° N	3580	13
42056	85.1° W	19.9° N	4562	13
42058	75.1° W	15.1° N	4195	12
42059	67.5° W	15.0° N	4863	11
42060	63.5° W	16.5° N	1436	9
44004	70.4° W	38.5° N	3140	13

79 the envelope of a group of irregular waves is derived from the radian wave  
80 frequency  $\omega = 2\pi f$  and wave number  $k$  as

$$c_g = \frac{\partial \omega}{\partial k} . \quad (2)$$

81 For deep waters ( $d/(gT^2) > 10^{-3}$  with  $d$  the water depth and  $T$  the wave pe-  
 82 riod) and small amplitude waves ( $H_s/(gT^2) < 10^{-3}$ ), the linear wave theory  
 83 applies resulting in the linear dispersion relationship [17]

$$\omega^2 = gk \tanh(kd) . \quad (3)$$

84 Combining Eqs. 2 and 3, the wave group velocity is expressed as

$$c_g = \frac{\omega}{2k} \left( 1 + \frac{2kd}{\sinh(2kd)} \right) . \quad (4)$$

85 In deep waters ( $kd \gg 1$ ), the group velocity is approximated as  $c_g = g/(2\omega)$   
 86 (from expression 4 by including the wave number formulation derived from  
 87 the linear dispersion equation 3) which results in the following relationship  
 88 for the available wave energy flux

$$P_1 = \frac{\rho g^2}{4\pi} \int_0^\infty \frac{E(f)}{f} df . \quad (5)$$

89 Eq. 5 is more generally rewritten as a function of the significant wave height  
 90  $H_s = 4\sqrt{m_0}$  and the wave energy period  $T_e = m_{-1}/m_0$  as

$$P_1 = \frac{\rho g^2}{64\pi} H_s^2 T_e \quad (6)$$

91 with  $m_n = \int_0^\infty f^n E(f) df$  the  $n^{th}$  order spectral moment.  $T_e$ , denoted the  
 92 wave energy period, represents the period of a single sinusoidal wave that  
 93 integrates the same amount of energy as in the real sea state.

94 However, the available hindcast archives are typically limited to bulk pa-  
 95 rameters that do not include the wave energy period and integrate informa-  
 96 tion on the spectral energy density in a reduced number of points (typically  
 97 wave buoys). The peak period was thus retained as being more available in

98 measurements and numerical hindcast databases than other statistical peri-  
 99 ods such as the spectral mean or zero-upcrossing periods. In this situation,  
 100 the wave energy period is determined from the available peak wave period  
 101 by introducing a calibration coefficient  $\alpha$  as  $T_e = \alpha T_p$ , which results in the  
 102 following formulation of the wave power density

$$P_2 = \frac{\rho g^2}{64\pi} H_s^2 \alpha T_p . \quad (7)$$

103 The calibration coefficient ( $\alpha$ ) is generally estimated by assuming stan-  
 104 dard shapes of the wave energy spectrum. It is set to (i)  $\alpha = 0.9$  for a  
 105 standard JONSWAP spectrum with a peak enhancement  $\gamma = 3.3$  [11, 12, 13]  
 106 and (ii)  $\alpha = 0.86$  for a Pierson-Moskowitz spectrum [18]. However, fur-  
 107 ther uncertainties exist in relation to the deformation of the wave energy  
 108 spectrum in coastal seas with values that vary between 0.86 (for wide-band  
 109 spectra) and 1 (for narrow-band spectra) [11]. Increased differences are fur-  
 110 thermore expected in combined sea states including long-crested swell and  
 111 short-crested wind-sea waves. Indeed, in this situation, the wave spectrum is  
 112 typically characterized by two energy maxima, in high and low frequencies,  
 113 and the peak period appears as a rough approximation of the wave energy  
 114 period. A wide range of  $\alpha$  values was thus obtained from the exploitation  
 115 of real sea states measurements. In a preliminary assessment of the wave  
 116 energy resource in Cape Verde islands (central Atlantic Ocean), Hagerman  
 117 [19] considered the wave energy period as being equal to the peak period. In  
 118 a revised assessment of the wave energy resource around Australia, Hemer  
 119 et al. [20] estimated this coefficient as  $\alpha = 0.857$ . By exploiting measure-  
 120 ments off Ireland in the Atlantic Marine Energy Test Site, Sheng and Li [21]  
 121 proposed to retain a coefficient  $\alpha = 0.8$  for spectra with two wave energy

122 peaks. More recently, Ahn et al. [22] analytically derived values of  $\alpha = 0.86$   
 123 for wind sea and  $\alpha = 1.0$  for swell.

124 The calibration coefficient ( $\alpha$ ) was furthermore established between  $T_p$   
 125 and  $T_e$ , disregarding the influence of  $H_s^2$  on wave power assessment. This  
 126 explains why this coefficient may differ from the value that ensures the best  
 127 fit between the spectral formulation (considered as the reference evaluation)  
 128 (Eq. 1) and the peak-period formulation (Eq. 7). As classes of  $H_s$  and  $T_p$  are  
 129 evolving in relation to sea states conditions, increased temporal variability  
 130 of  $\alpha$  is also expected. Whereas the error associated with this calibration  
 131 coefficient is less important for wave power computation than the squared  
 132 error on the significant wave height, refined investigations are finally required  
 133 to assess the variability of this coefficient against sea wave conditions focusing  
 134 on its evolution at monthly, seasonal and annual time scales.

### 135 2.3. Wave exploitation

136 The available wave energy flux was successively computed with Eqs. 1, 6  
 137 and 7. In all cases, formulations were applied to a finite number of observed  
 138 spectral energy density components  $E_i = E(f_i)$  displayed in  $n$  frequencies  $f_i$   
 139 with  $i \in [1, n]$ . The initial spectral formulation (Eq. 1) was thus expressed  
 140 as

$$P_{spectral} = \rho g \sum_{i=1}^{n-1} \frac{1}{2} (c_{g,i} E_i + c_{g,i+1} E_{i+1}) (f_{i+1} - f_i) \quad (8)$$

141 with  $c_{g,i} = c_g(f_i)$  the group velocity obtained for frequency  $f_i$  with Eq. 4.  
 142 An iteration process was applied to obtain the wave number from the linear  
 143 dispersion relationship (Eq. 3). The wave parameters  $H_s = 4\sqrt{m_0}$  and  
 144  $T_e = m_{-1}/m_0$  were computed, in a similar manner, from the evaluation of

145 spectral moments  $m_0$  and  $m_{-1}$  estimated as

$$m_0 = \sum_{i=1}^{n-1} \frac{1}{2} (E_i + E_{i+1}) (f_{i+1} - f_i) \quad (9)$$

146 and

$$m_{-1} = \sum_{i=1}^{n-1} \frac{1}{2} \left( \frac{E_i}{f_i} + \frac{E_{i+1}}{f_{i+1}} \right) (f_{i+1} - f_i) \quad (10)$$

147 The peak period was finally evaluated from the frequency bin characterizing  
148 the wave energy peak. These wave parameters were integrated in Eqs. 6  
149 and 7 to obtain the available wave power densities  $P_1$  and  $P_2$ . The peak-  
150 period formulation was applied with a default calibration coefficient  $\alpha = 0.9$   
151 assuming JONSWAP shape of the wave energy spectrum (Section 2.2). This  
152 resulted in three consistent evaluations of the wave power density based on  
153 (i) the spectral energy density (Eq. 1), (ii)  $H_s$  and  $T_e$  (Eq. 6), and (iii)  $H_s$   
154 and  $T_p$  (Eq. 7).

### 155 3. Results and discussion

#### 156 3.1. Mean wave power density

157 Before evaluating the wave power density, computed values of  $H_s$  and  $T_p$   
158 were compared with the standard meteorological data provided after process-  
159 ing of wave energy spectrum by NDBC [16]. These comparisons confirmed  
160 the reliability of the method retained in the present investigation to compute  
161 wave parameters from energy spectrum (Section 2.3).

162 The attention was first dedicated to the estimation of the mean available  
163 wave energy flux commonly evaluated in the preliminary stages of a wave  
164 energy project (Fig. 2-a). These mean values were computed by averaging  
165 the estimations of wave power density during the duration of wave buoys

166 observations. Whereas these estimations concerned different periods of time,  
 167 results obtained were consistent with worldwide and local resource assess-  
 168 ments [3, 12, 23, 24, 25] exhibiting, with the spectral density formulation  
 169 1, values between 15 and 25  $\text{kWm}^{-1}$  in the offshore areas that reduced be-  
 170 low 10  $\text{kWm}^{-1}$  in the less exposed regions of the Gulf of Mexico and the  
 171 Caribbean Sea. A slight increase of wave power density, up to values of  
 172 13  $\text{kWm}^{-1}$  was, however, identified in the Carribbean Sea (point 42058) in  
 173 relation to the influence of the Caribbean Low-Level Jet, an easterly zonal  
 174 wind liable to reach 13  $\text{ms}^{-1}$  [25]. These evaluations at measurement points  
 175 appeared furthermore in the range of values obtained by Defne et al. [14],

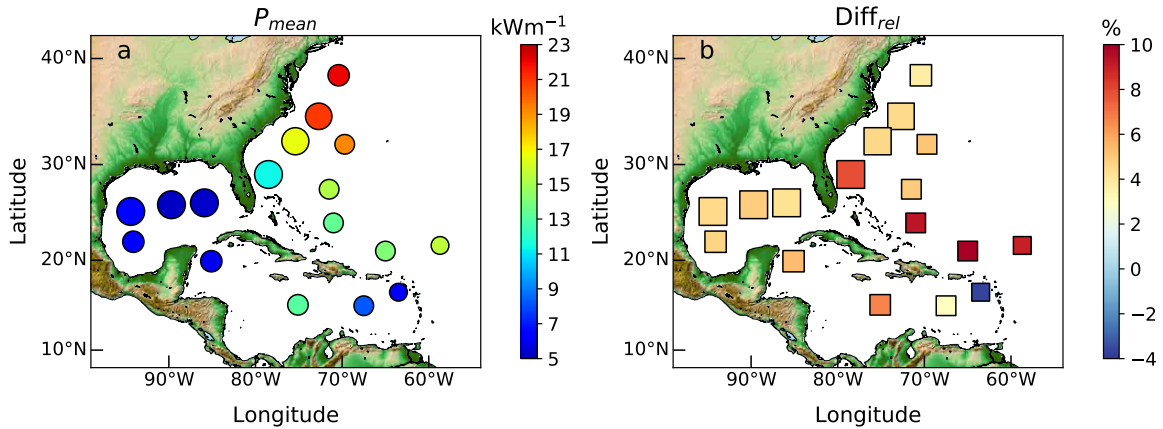


Figure 2: (a) Mean available wave energy flux at measurement points computed with the spectral density formulation 1 and (b) relative differences with respect to the evaluation based on the peak-period (formulation 7)  $Diff_{rel} = 100(\bar{P}_2 - \bar{P}_{spectral})/\bar{P}_{spectral}$  with the overbar denoting the averaged values. Circles diameters were set proportional to the duration of observations. Positive values account for an overestimation of the wave power density with the peak-period formulation 7 while negatives values exhibit an underestimation of the available wave energy flux.

176 off the USA East Coast, at wave buoys 41001, 41002 and 41010 by applying  
177 a moving average filter to wave power observations.

178 Confirming the approximation of the group velocity in deep waters (Sec-  
179 tion 2.2), the relationship based on the energy period (Eq. 6) provided nearly  
180 the same values of the mean wave power density than the spectral formulation  
181 (Eq. 1). As exhibited by scatter plot results of the available wave energy flux  
182 at the different time steps (illustration provided at point 41046 in Fig. 3),  
183 this energy-period formulation appeared as a very good approximation of the  
184 wave energy flux in deep waters promoting the output of  $T_e$  in numerical re-  
185 source assessments. This results contrasted, however, with the investigation  
186 conducted by Ozkan and Mayo [15] that exhibited an underestimation of the  
187 wave power density by an average of 17% with the energy-period formulation  
188 6 off the Florida Peninsula. Whereas wave buoys considered by Ozkan and  
189 Mayo [15] were located in reduced water depths with associated modulation  
190 of the group velocity, this tendency was also obtained at point 42003 by more  
191 than 3200 m of water depths where the formulation 4 for the group velocity  
192 should mathematically converge to  $c_g = g/(2\omega)$ . As exhibited in the present  
193 investigation, reduced differences should thus be obtained in this location  
194 between the spectral formulation 1 and the energy-period formulation 6.

195 The formulation based on the peak period (Eq. 7 with a standard calibra-  
196 tion coefficient  $\alpha = 0.9$ ) resulted, however, in increased differences (Fig. 2-b).  
197 With an exception at point 42060, this approximation was found to overesti-  
198 mate the mean available wave energy flux at all measurement locations with  
199 differences ranging from 3 – 5% in the Gulf of Mexico and the northern part  
200 of USA East Coast to 7 – 10% off Florida Peninsula, the Bahamas and the

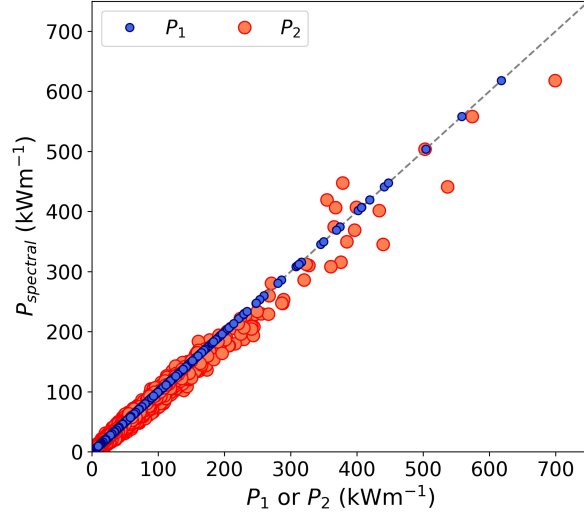


Figure 3: Scatter plot results of  $P_{spectral}$  against  $P_1$  and  $P_2$  at wave buoy 41046 (Fig. 1 and Table 1).

201 Greater Antilles.

### 202 3.2. Wave power variability

203 However, the mean wave power density is a bulk parameter that provides  
 204 very limited information about the variability of the wave climate and asso-  
 205 ciated uncertainties in power generation, both aspects that are very critical  
 206 for determining the location of energy converters in the marine environment  
 207 [2, 4]. For these reasons, differences obtained between wave power formula-  
 208 tions were successively exhibited at the annual, seasonal and monthly time  
 209 scales.

210 Time series of yearly-averaged available wave energy flux were first com-  
 211 puted at measurement points for years that contained more than 95% of ob-  
 212 servations. Results obtained confirmed the tendency of formulation 7 (with a

213 calibration coefficient  $\alpha = 0.9$ ) to overestimate the wave power density with  
 214 differences liable to reach 10% in 2010 at point 41044, off the Lesser Antilles  
 215 (Fig. 4). These relative differences were averaged at every measurement  
 216 locations to provide a global estimation of uncertainties associated with the  
 217 peak-period formulation by adopting the following relationship

$$\text{Diff}_{rel,year} = \frac{1}{n_{year}} \sum_{i=year1}^{year2} 100 \frac{(\bar{P}_{2,i} - \bar{P}_{spectral,i})}{\bar{P}_{spectral,i}} \quad (11)$$

218 with the overbar denoting the yearly-averaged values and  $n_{year}$  the number  
 219 of years that integrated more than 95% of observations between  $year1$  and  
 220  $year2$ . The resulting spatial distribution (Fig. 5) appeared consistent with  
 221 the analysis conducted on the mean available wave energy flux (Fig. 2) with  
 222 differences up to 9% off the Greater Antilles.

223 Time series of monthly-averaged available wave power density were then  
 224 evaluated at measurement points for years containing more than 95% of data,  
 225 this in order to gain further insights about the variation of differences at the  
 226 seasonal time scale (Fig. 6). With an exception at point 42058 characterized  
 227 by summer energetic conditions associated to the influence of the Caribbean  
 228 Low-Level Jet [25], a clear contrast was exhibited at measurement locations  
 229 between (i) winter months with the highest energetic values and (ii) summer  
 230 months with reduced energy levels. Increased absolute differences (between  
 231 the peak-period formulation 7 and the spectral formulation 1) were naturally  
 232 obtained during the most energetic months. However, these differences ac-  
 233 counted for nearly the same proportion of the available wave power density  
 234 during a year (Fig. 7). Whereas a slight increase of these relative differences  
 235 was exhibited during the winter and spring periods, the spatial distribution  
 236 retained the same patterns with an averaged overestimation of wave power

237 density between 8 and 10% in the western part of Florida Peninsula, and off  
 238 the Bahamas and the Greater Antilles that reduced below 5% in the Gulf of  
 239 Mexico, the Caribbean Sea and the northern part of USA East Coast.

### 240 3.3. Calibration coefficient

#### 241 3.3.1. Spatio-temporal variations

242 Whereas the energy-period formulation 6 appeared as a very good approx-  
 243 imation of the wave power density in deep waters, the peak-period formula-  
 244 tion 7 exhibited further differences. This latter formulation was applied with  
 245 a standard calibration coefficient  $\alpha = 0.9$  by assuming JONSWAP shapes for  
 246 the wave energy spectrum (Section 2.2). Variations of this coefficient were  
 247 thus expected with respect to the distribution of wave energy among fre-

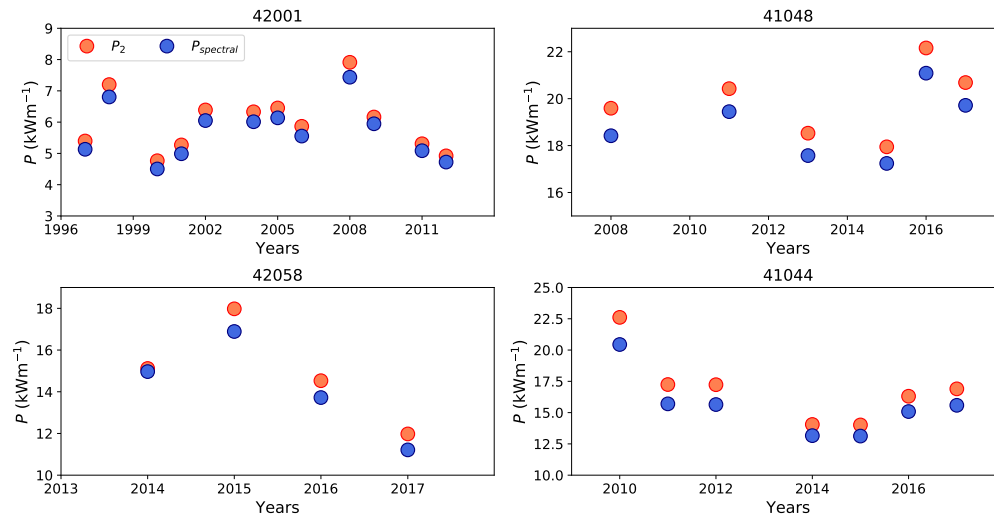


Figure 4: Yearly-averaged available wave energy flux at points 42001, 41048, 42058 and 41044 obtained with the spectral formulation 1 and the peak-period formulation 7 (with a default coefficient  $\alpha = 0.9$ ). The available wave energy flux was computed for years that integrated more than 95% of observations.

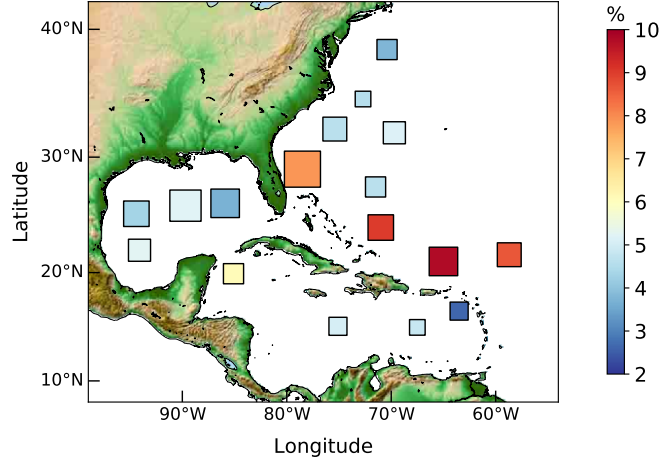


Figure 5: Relative differences,  $\text{Diff}_{rel,year}$ , in the estimation of yearly-averaged available wave energy flux between the peak-period formulation 7 (with  $\alpha = 0.9$ ) and the spectral formulation 1. The computation was performed for years that contained more than 95% of observations.

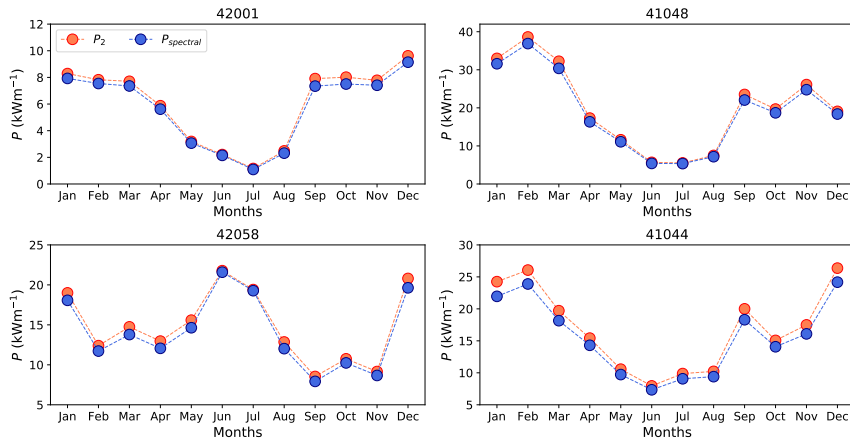


Figure 6: Monthly-averaged available wave energy flux at points 42001, 41048, 42058 and 41044 obtained with the spectral formulation 1 and the formulation 7 based on the peak period. Data were computed for years that integrated more than 95% of observations.

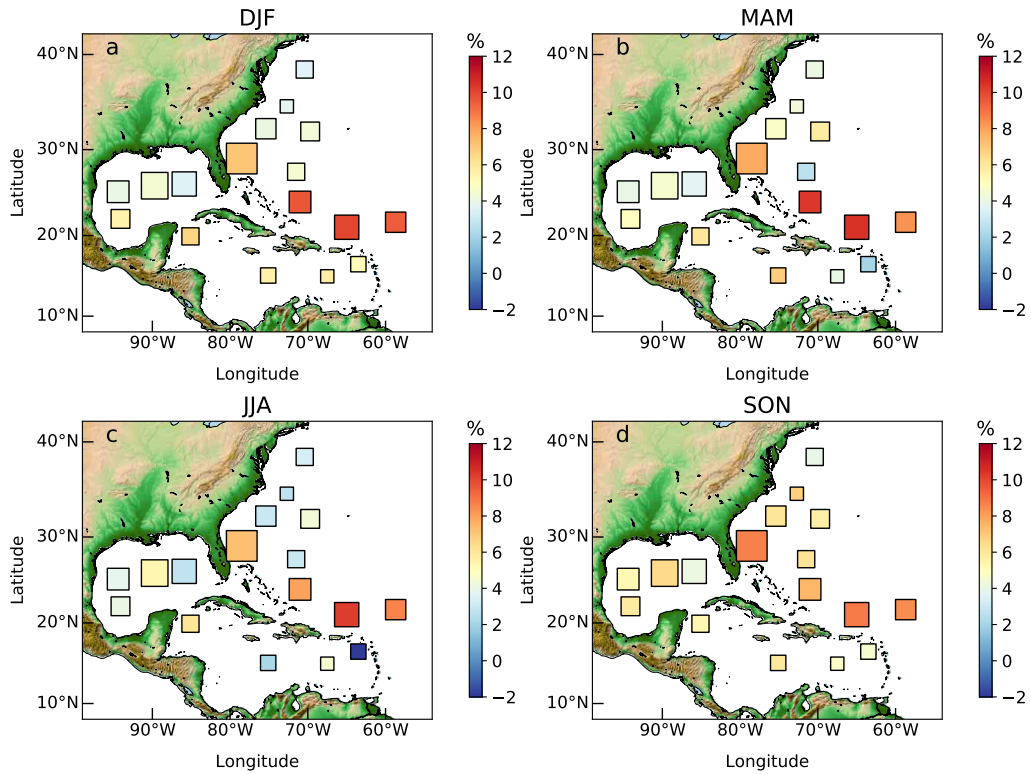


Figure 7: Relative seasonal differences in the estimation of the averaged available wave energy flux between the peak-period formulation 7 and the spectral formulation 1. The four seasons were defined with respect to three-month seasonal time scale as (a) winter (December, January and February), (b) spring (March, April and May), (c) summer (June, July and August) and (d) autumn (September, October and November). The computation was performed for years that contained more than 95% of observations.

248 quencies, especially in conditions of combined long-crested swell and locally  
 249 generated wind sea. As  $P_1$  was nearly equal to  $P_{spectral}$ ,  $\alpha$  that was defined  
 250 as the ratio between  $T_e$  and  $T_p$  (Section 2.2) could also be interpreted as the  
 251 ratio between  $P_{spectral}$  and  $P_2 = \rho g^2 / (64\pi) H_s^2 T_p$  in deep waters. The calibra-  
 252 tion coefficient was thus directly analyzed with respect to the computations  
 253 of available wave energy flux.

254 However, it was very difficult to retain, at all measurement locations, a  
 255 constant coefficient that optimized the estimation of the wave power density  
 256 with the peak-period formulation 7. Adjusting  $\alpha$  to provide the best estimate  
 257 of the mean available wave energy flux (initially displayed in Fig. 2) provided  
 258 thus values varying between 0.82 and 0.93 (Fig. 8). Lowest values ( $\alpha < 0.84$ )  
 259 were obtained in areas (off Florida Peninsula, the Bahamas, the Greater

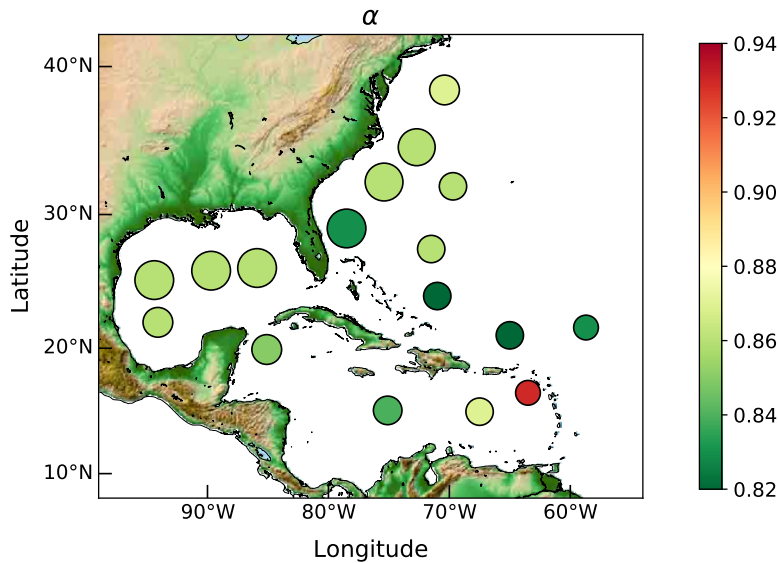


Figure 8: Calibration coefficient that provided the best evaluation of the mean available wave energy flux with the peak-period formulation 7.

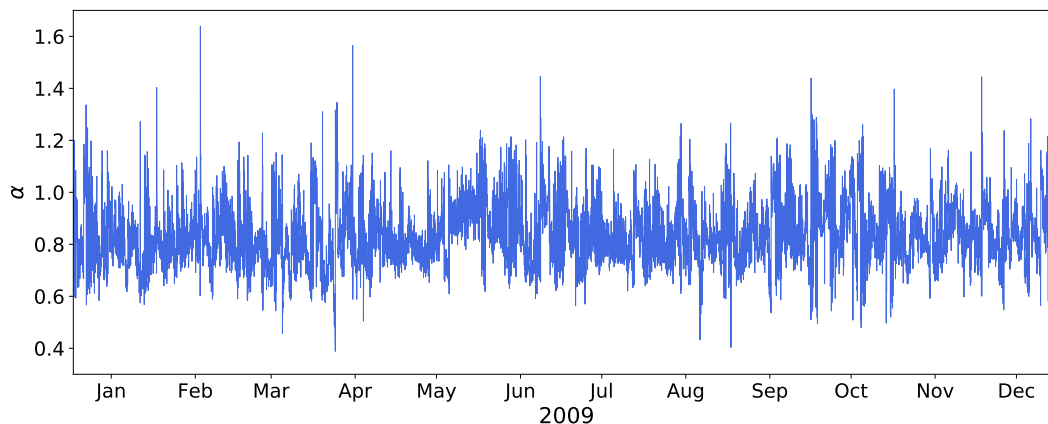


Figure 9: Time series of the calibration coefficient  $\alpha$  at point 41046 in 2009.

260 Antilles and USA East Coast) initially characterized by the more important  
 261 overestimation of the wave power density while the highest value (up to  
 262 0.93) was computed at point 42060 that exhibited an underestimation of the  
 263 available power. In a given location,  $\alpha$  was furthermore characterized by  
 264 significant variations (between 0.4 and 1.7 at wave buoy 41046, Fig. 9), well  
 265 beyond the range of values previously identified.

### 266 3.3.2. Distribution against $H_s$ and $T_p$

267 Nevertheless, as exhibited at wave buoy 41046 (Fig. 10), the calibration  
 268 coefficient was found to follow tendencies with respect to the significant wave  
 269 height  $H_s$  and the peak period  $T_p$ .  $\alpha$  was thus found to converge for the  
 270 most energetic sea states whereas more dispersion was obtained in reduced  
 271 energy levels with calibration coefficients decreasing as the peak period was  
 272 increasing. This dispersion of  $\alpha$  in reduced-energetic sea states was attributed  
 273 to two types of wave conditions, (i) dominated by swell (Fig. 11-a) and  
 274 (ii) resulted from the combination of swell and locally generated wind sea

275 (Fig. 11-b). In the first type (Fig. 11-a), swell dominated the wave  
 276 energy spectrum and the peak period was higher than the energy period  
 277 ( $T_p = 11.4$  s /  $T_e = 6.5$  s in the illustration) which resulted in reduced values  
 278 of the calibration coefficient ( $\alpha = 0.57$ ). In the second type (Fig. 11-b),  
 279 the energy of locally-generated wind seas competed with or dominated the  
 280 swell energy, and the peak period was reduced ( $T_p = 5.9$  s) which increased  
 281 the calibration coefficient ( $\alpha = 1.27$ ). This tendency was identified at the 17  
 282 measurement locations and exhibited with the distribution of averaged values  
 283 of  $\alpha$  in classes of  $H_s$  and  $T_p$  at the four points 42001, 41048, 42058 and 41044  
 284 located in the Gulf of Mexico, the Caribbean Sea, and the oceanic regions  
 285 off the USA East Coast, the Bahamas and the Antilles (Fig. 12). Whereas  
 286 the calibration coefficient of a given  $H_s/T_p$  class varied between these four  
 287 locations, it exhibited overall similar distributions against significant wave

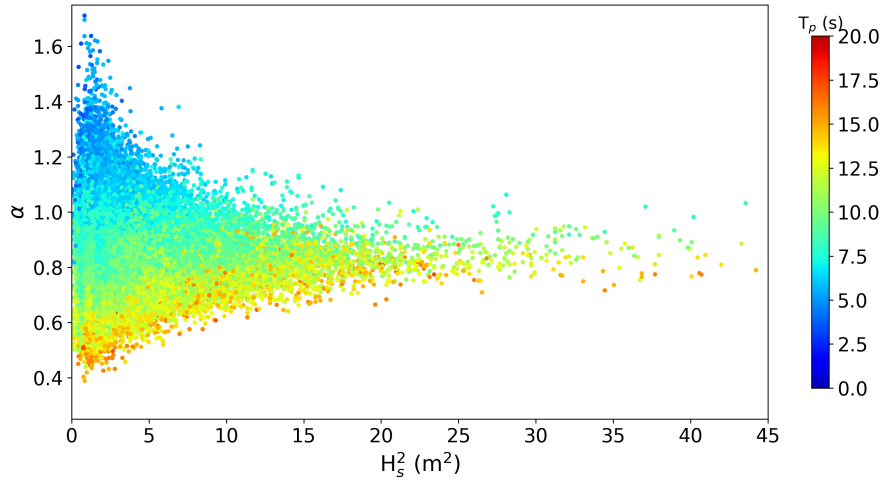


Figure 10: Evolution of the calibration coefficient  $\alpha$  with respect to the significant wave height squared and the peak period at point 41046.

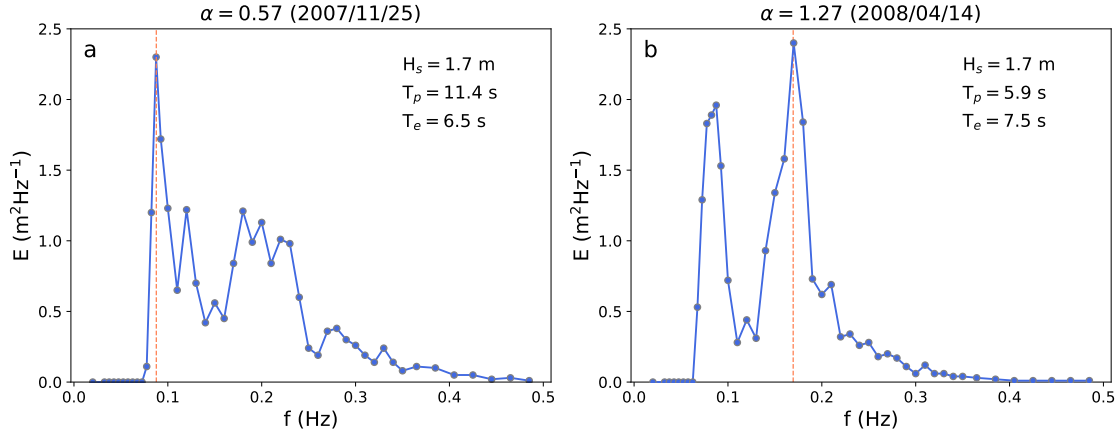


Figure 11: Spectral energy density  $E$  with respect to the frequency at point 41046 for conditions of (a)  $\alpha = 0.57$  and (b)  $\alpha = 1.27$ . The vertical line shows the peak frequency.

288 height and peak period.  $\alpha$  was thus found to (i) converge to values between  
 289 0.8 and 0.9 for the most energetic sea states, (ii) increase to values over 1.1  
 290 in reduced energetic conditions dominated by locally-generated wind seas  
 291 and (iii) decrease to values below 0.6 in low energetic swell conditions. The  
 292 distribution of calibration coefficients in low energetic conditions contrasted,  
 293 however, with the values computed by Ahn et al. [22] ( $\alpha = 0.86$  for wind sea  
 294 against  $\alpha = 1.0$  for swell). These differences may be attributed to the shape  
 295 of the energy spectrum retained by Ahn et al. [22] to derive these coefficients  
 296 (based on Pierson-Moskowitz spectrum for wind sea and Gaussian spectrum  
 297 for swell) with single energy peak, only.

298 On the basis of the distributions of calibration coefficients, a simplified  
 299 method was proposed to reduce the biases associated with the peak-period  
 300 formulation 7. Matrices of calibration coefficients computed at the 17 mea-  
 301 surement locations were first agglomerated in a single matrix that encom-

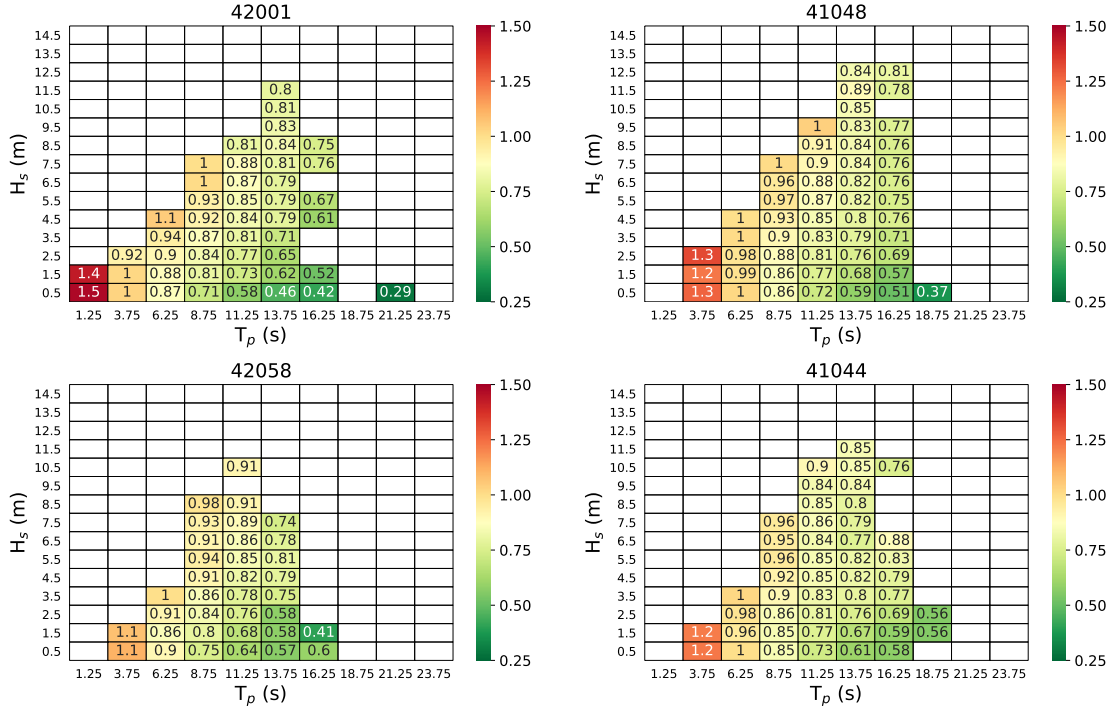


Figure 12: Distribution of the calibration coefficient  $\alpha$  in classes of  $H_s$  and  $T_p$  at wave buoys 42001, 41048, 42058 and 41044.

302 passed the overall distribution of  $\alpha$  against  $H_s$  and  $T_p$  (Fig. 13). The peak-  
 303 period formulation was then applied by evaluating the calibration coefficient  
 304  $\alpha$  with this matrix based on values of  $H_s$  and  $T_p$ , only. This original com-  
 305 putational method (restricted to the knowledge of a single distribution of  $\alpha$   
 306 coefficients) improved the estimation of the available wave energy flux at the  
 307 measurement locations. Scatter plots results of  $P_{spectral}$  against  $P_2$  (based  
 308 on  $T_p$ ) illustrated these improved estimations, particularly noticeable in the  
 309 highest energetic sea states (Fig. 14). With an exception at point 42060  
 310 located in the vicinity of the Lesser Antilles, the new method resulted fur-

311 thermore in better evaluations of the mean available wave power density (Fig.  
 312 15-a). The improvement was particularly noticeable in oceanic wave buoys  
 313 off the USA East Coast, the Bahamas and the Antilles. The relative differ-  
 314 ence was thus decreasing from 9.9% to 0.3% at point 41043 off the Greater  
 315 Antilles. In spite of increased differences at points 41047, 42055 and 42059  
 316 in spring and summer, the new method improved finally the estimations of  
 317 temporal variations of wave power at annual and seasonal time scales (Figs.  
 318 15-b and 16).

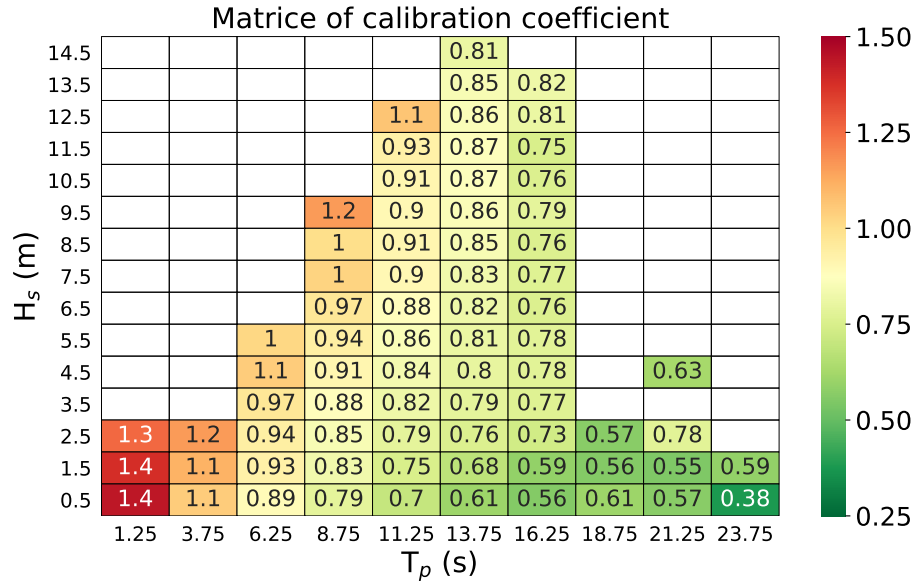


Figure 13: Distribution of the calibration coefficient  $\alpha$  in classes of  $H_s$  and  $T_p$  resulting from the integration of all observations at the 17 wave buoys.

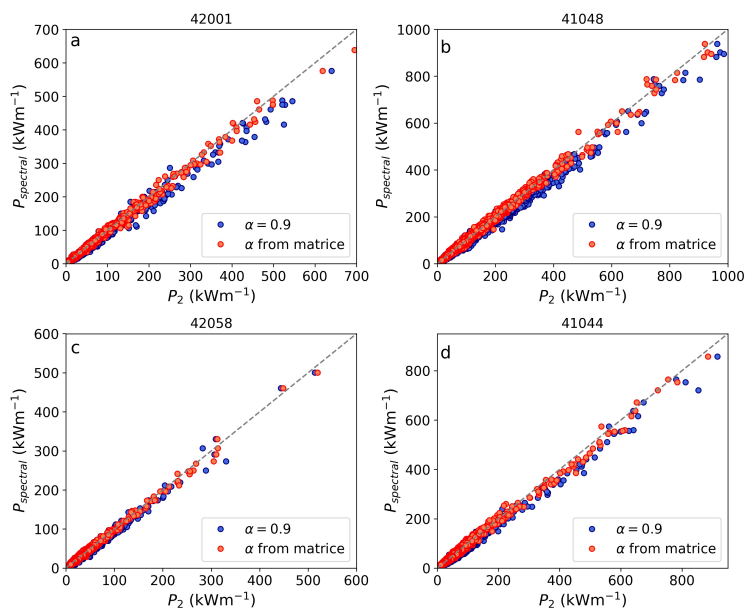


Figure 14: Scatter plot results of  $P_{spectral}$  against  $P_2$  with (i) the default calibration coefficient  $\alpha = 0.9$  and (ii) the calibration coefficient matrix displayed in Fig. 13 at wave buoys 42001, 41048, 42058 and 41044.

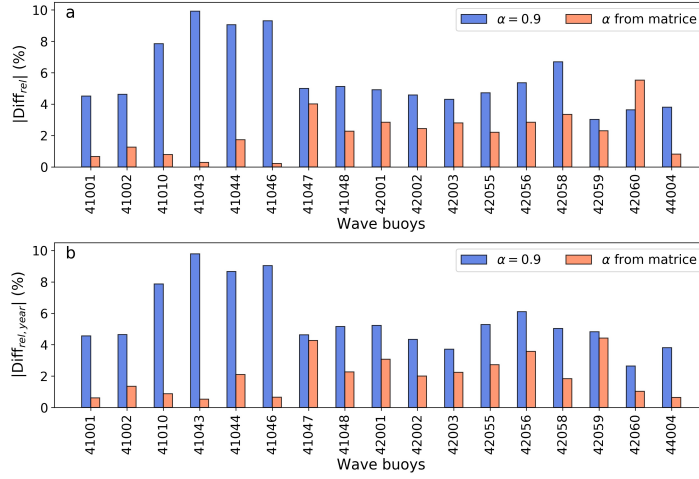


Figure 15: Comparison of the absolute values of the relative differences (a)  $|\text{Diff}_{rel}|$  (Fig. 2) and (b)  $|\text{Diff}_{rel,year}|$  (Fig. 5) in measurement locations with the peak-period formulation based on (i) the default calibration coefficient  $\alpha = 0.9$  and (ii) the calibration coefficient matrix displayed in Fig. 13.

#### 319 4. Conclusion

320 Long-term observations of wave conditions were exploited in 17 wave  
 321 buoys located in mean water depths over 600 m in the North-West Atlantic,  
 322 the Gulf of Mexico and the Caribbean Sea to assess differences associated  
 323 with simplified formulations of the available wave energy flux based on the  
 324 energy period and the peak period. The main outcomes of the present study  
 325 are as follows:

- 326 1. The energy-period formulation 6 based on the approximation of the  
 327 group velocity in deep waters provided a very good evaluation of the  
 328 available wave power density and promoted the output of the energy  
 329 period in numerical hindcast evaluations of wave conditions.

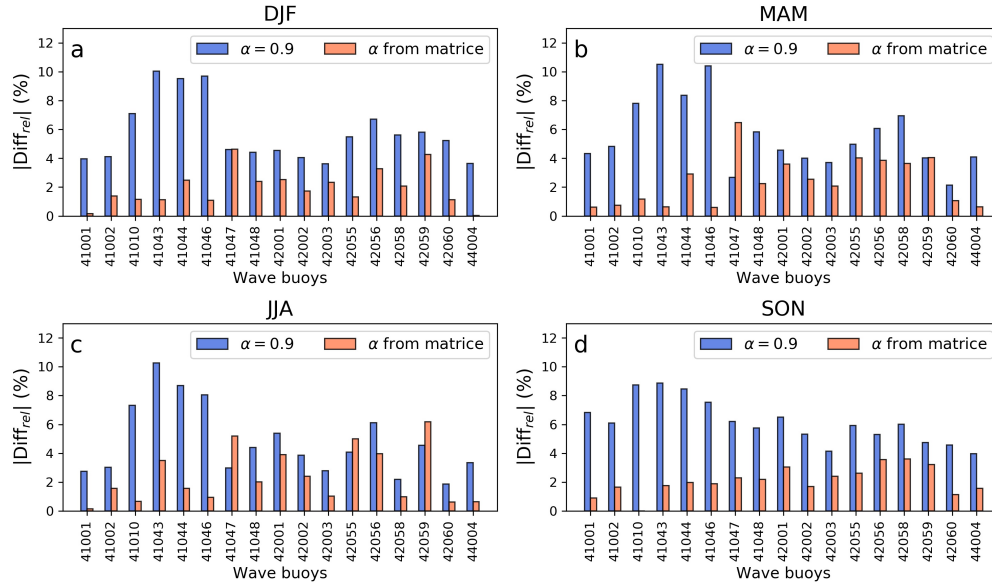


Figure 16: Comparison of the absolute values of the relative differences in the estimation of the averaged available wave energy flux in (a) winter, (b) spring, (c) summer and (d) autumn with the peak-period formulation based on (i) the default calibration coefficient  $\alpha = 0.9$  and (ii) the calibration coefficient matrix displayed in Fig. 13.

- 330 2. The peak-period formulation 7 parameterized with a default calibration  
 331 coefficient  $\alpha = 0.9$  (matching JONSWAP shape of the wave energy  
 332 spectrum) exhibited increased differences with a tendency to overes-  
 333 timate the available wave energy flux by more than 8% off Florida  
 334 Peninsula, the Bahamas and the Greater Antilles.
- 335 3. The calibration coefficient was characterized by important spatial and  
 336 temporal variations. Optimizing this coefficient to provide the best  
 337 evaluation of the mean available wave power density resulted in values  
 338 varying between 0.82 and 0.93. This coefficient exhibited furthermore  
 339 increased variations between 0.4 and 1.7 when focusing on its temporal

340 evolution at a given location.

- 341 4. The calibration coefficient followed, however, tendencies with respect to  
342 classes of significant wave height and peak period. While  $\alpha$  was found to  
343 converge to values around 0.8 and 0.9 for the most energetic sea states,  
344 increased dispersion was obtained in reduced energetic conditions. For  
345 these reduced energetic levels,  $\alpha$  decreased thus to values below 0.6 in  
346 swell-dominated conditions and reached values over 1.1 in combined  
347 swell and locally-generated wind sea.
- 348 5. A refined distribution of  $\alpha$  against classes of  $H_s$  and  $T_p$  was finally  
349 established by agglomerating the long-term observations of wave con-  
350 ditions in measurement locations. This single matrix was integrated in  
351 the simplified formulation of the available wave power density based on  
352 the peak period. Significant improvements were reached for the eval-  
353 uation of the averaged values at annual, seasonal and monthly time  
354 scales.

355 Further investigations are naturally required to refine the estimation of the  
356 distribution of  $\alpha$  against classes of  $H_s$  and  $T_p$ , and assess the robustness of  
357 this original method. However, results obtained suggested to rely on varying  
358 calibration coefficients to improve the evaluations of the available wave energy  
359 flux by exploiting available hindcast predictions and/or observations of  $H_s$   
360 and  $T_p$ . This method may thus be tested in different oceanic conditions such  
361 as the USA West Coast where a series of observations is made available by the  
362 National Data Buoy Center. It would furthermore be interesting to analyze  
363 the application of this technique in nearshore water depths characterized by  
364 different assumptions of the group velocity and reliability of the approach

365 based on the energy period.

## 366 **Acknowledgements**

367 In-situ observations were provided by the National Oceanic and Atmo-  
368 spheric Administration (NOAA). The present paper is a contribution to  
369 the research program DIADEME (“Design et InterActions des Dispositifs  
370 d’extraction d’Energies Marines avec l’Environnement”) of the Laboratory  
371 of Coastal Engineering and Environment (Cerema, <http://www.cerema.fr>).

## 372 **References**

- 373 [1] A. Falcão, Wave energy utilization: a review of the technologies, Re-  
374 newable & Sustainable Energy Reviews 14 (2010) 899–918.
- 375 [2] S. Neill, M. Hashemi, Wave power variability over the northwest Euro-  
376 pean shelf seas, Applied Energy 106 (2013) 31–46.
- 377 [3] J. Portilla, J. Sosa, L. Cavaleri, Wave energy resources: Wave climate  
378 and exploitation, Renewable Energy 57 (2013) 594–605.
- 379 [4] N. Guillou, G. Chapalain, Annual and seasonal variabilities in the per-  
380 formances of wave energy converters, Energy 165 (2018) 812–823.
- 381 [5] N. Guillou, G. Chapalain, Numerical modelling of nearshore wave energy  
382 resource in the Sea of Iroise, Renewable Energy 83 (2015) 942–953.
- 383 [6] M. Gonçalves, P. Martinho, C. G. Soares, A 33-year hindcast on wave  
384 energy assessment in the western French coast, Energy 165 (2018) 790–  
385 801.

- 386 [7] S. Gallagher, R. Tiron, F. Dias, A long-term nearshore wave hindcast  
387 for Ireland: Atlantic and Irish Sea coasts (1979-2012), *Ocean Dynamics*  
388 64 (2014) 1163–1180.
- 389 [8] C. Appendini, A. Torres-Freyermuth, J. López-González, E. T. Men-  
390 doza, Wave Climate and Trends for the Gulf of Mexico: A 30-Yr Wave  
391 Hindcast, *Journal of Climate* 27 (4) (2014) 1619–1632.
- 392 [9] W. Pierson, L. Moskowitz, A proposed spectral form for fully developed  
393 wind seas based on the similarity theory of S.A. Kitaigorodskii, *Journal*  
394 *of Geophysical Research* 69 (24) (1964) 5181–5190.
- 395 [10] K. Hasselmann, T. Barnett, E. Bouws, H. Carlson, D. Cartwright,  
396 K. Ende, J. Ewing, H. Gienapp, D. Hasselmann, P. Kruseman, A. Meer-  
397 burg, P. Muller, D. Olbers, K. Richter, W. Sell, H. Waldden, Measure-  
398 ments of wind-wave growth and swell decay during the JOint North Sea  
399 WAVE Project (JONSWAP), *Dtsch. Hydrogr. Z. Suppl.* 12 (A8) (1973)  
400 1–95.
- 401 [11] J. Sierra, A. White, C. Mösso, M. Mestres, Assessment of the intra-  
402 annual and inter-annual variability of the wave energy resource in the  
403 Bay of Biscay (France), *Energy* 141 (2017) 853–868.
- 404 [12] A. Cornett, A global wave energy resource assessment, in: *Proceedings*  
405 *of the International Journal of Offshore and Polar Engineering*, 2008.
- 406 [13] J. Pastor, Y. Liu, Wave Climate Resource Analysis Based on a Revised  
407 Gamma Spectrum for Wave Energy Conversion Technology, *Sustain-*  
408 *ability* 8 (1321) (2016) –.

- 409 [14] Z. Defne, K. A. Haas, H. M. Fritz, Wave power potential along the  
410 Atlantic coast of the southeastern USA, *Renewable Energy* 34 (2009)  
411 2197–2205.
- 412 [15] C. Ozkan, T. Mayo, The renewable wave energy resource in coastal  
413 regions of the Florida peninsula, *Renewable Energy* 139 (2019) 530–537.
- 414 [16] NDBC, [https://www.ndbc.noaa.gov/historical\\_data.shtml](https://www.ndbc.noaa.gov/historical_data.shtml), 2019.
- 415 [17] L. Holthuijsen, *Waves in Oceanic and Coastal Waters*, Cambridge Uni-  
416 versity Press, Cambridge, 2007.
- 417 [18] F. Arena, V. Laface, G. Malara, A. Romolo, A. Viviano, V. Fiamma,  
418 G. Sannino, A. Carillo, Wave climate analysis for the design of wave  
419 energy harvesters in the Mediterranean Sea, *Renewable Energy* 77 (2015)  
420 125–141.
- 421 [19] G. Hagerman, Southern New England Wave Energy Resource Potential,  
422 in: *Proc. Building 23 Energy’2011*, Boston, USA, 2001.
- 423 [20] M. Hemer, S. Zieger, T. Durrant, J. O’Grady, R. Hoeke, K. McInnes,  
424 U. Rosebrock, A revised assessment of Australia’s national wave energy  
425 resource, *Renewable Energy* 114 (2017) 85–107.
- 426 [21] W. Sheng, H. Li, A Method for Energy and Resource Assessment of  
427 Waves in Finite Water Depths, *Energies* 10 (460).
- 428 [22] S. Ahn, K. A. Haas, V. S. Neary, Wave energy resource classification sys-  
429 tem for US coastal waters, *Renewable and Sustainable Energy Reviews*  
430 104 (2019) 54–68.

- 431 [23] K. Gunn, C. Stock-Williams, Quantifying the global wave power re-  
432 source, *Renewable Energy* 44 (2012) 296–304.
- 433 [24] B. Reguero, I. Losada, F. Méndez, A global wave power resource and  
434 its seasonal, interannual and long-term variability, *Applied Energy* 148  
435 (2015) 366–380.
- 436 [25] C. Appendini, C. Urbano-Latorre, B. Figueroa, C. Dagua-Paz,  
437 A. Torres-Freyermuth, P. Salles, Wave energy potential assessment in  
438 the Caribbean Low Level Jet using wave hindcast information, *Applied*  
439 *Energy* 137 (2015) 375–384.